PHYSICAL REVIEW D **79,** 055001 (2009)

Single production of excited spin-3/2 neutrinos at linear colliders

O. Çakır* and A. Ozansoy†

Physics Department, Theory Division, CERN, 1211 Geneva 23, Switzerland
and Faculty of Sciences, Department of Physics, Ankara University, 06100, Tandogan, Ankara, Turkey

(Received 26 September 2008; published 2 March 2009)

We study the potential of future high energy e^+e^- colliders to probe excited neutrino signals in different channels coming from the single production process via gauge interactions. We calculate the production cross section, decay widths, and branching ratios of excited spin-3/2 neutrinos according to their effective currents and we compare them with those of the spin-1/2 ones. The signals and corresponding backgrounds are examined in detail to get accessible limits on the masses and couplings of excited spin-3/2 neutrinos.

DOI: 10.1103/PhysRevD.79.055001 PACS numbers: 12.60.Rc, 13.66.Hk, 13.85.Rm

I. INTRODUCTION

Phenomenologicaly, an excited lepton can be considered as a heavy lepton sharing leptonic quantum number (flavor) with the corresponding standard model (SM) lepton. Excited leptons (l^*) are suggested by a composite model of leptons [1,2]. The compositeness of leptons and quarks is characterized by a large mass scale Λ. The lepton compositeness would be the most pronounced in the excess of high-p_T events in the forthcoming high energy experiments. If leptons are composites, they can be assigned to spin-1/2 bound states, containing three spin-1/2 or spin-1/2 and spin-0 subparticles. Bound states and/or excited states of spin-3/2 leptons are possible with three spin-1/2 [1] or spin-1/2 and spin-1 subparticles in the framework of compositeness. Composite leptons in the enlarged groups of standard theory would also imply spin-3/2 leptons [3,4]. Further motivation for spin-3/2 particles comes from the supergravity where a spin-3/2 gravitino is the superpartner of the graviton [5]. Massive spin-3/2 excited neutrinos with the analogous heavy spin-1/2 excited ones can be produced at future high energy colliders through their effective interactions with the ordinary leptons. In the electron-positron collisions, pair production of excited spin-3/2 neutrinos can also be performed, but it is limited kinematically by $m^* < \sqrt{s}/2$, while single production can directly reach masses as high as $\sqrt{s}$. Furthermore, an excited neutrino could contribute to the pair production of charged weak bosons through its exchange in the t channel [6].

The mass limits for an excited spin-1/2 neutrino from its single production search are $m^* > 190$ GeV and $m^* > 102.6$ GeV from their pair production [7] assuming $f = -f'$, where f and f' are the scaling factors for the gauge couplings of $SU(2)$ and $U(1)$. Relatively small mass limits are obtained for $f = f'$. In this case, the mass limits for the excited spin-1/2 neutrinos are $m_{\nu_e^*} > 101.7$ GeV, $m_{\nu_\mu^*} > 101.8$ GeV, and $m_{\nu_\tau^*} > 92.9$ GeV [7]. Recently, a search for the excited spin-1/2 neutrinos has been performed by the H1 Collaboration [8] assuming $f = f'$ and $f/\Lambda = 1/m^*$, with an exclusion limit for the mass range of excited neutrino $m^* < 213$ GeV at 95% C.L.

Excited spin-1/2 leptons were studied at hadron colliders in [9–11] by taking into account possible backgrounds. Excited fermions have been studied at e^+e^- and ep colliders [12,13]. These studies have shown that excited spin-1/2 lepton masses up to 2 TeV can be probed at the CERN LHC. Our previous work on excited spin-3/2 electrons [14] shows that they can be distinguished from the spin-1/2 ones by analyzing the angular distribution of final state observable particles. This study is a continuation of the previous search for excited electrons [14]. An analysis of the production and decay processes of single heavy spin-3/2 neutrinos was performed in [15,16] in the frame of two phenomenological currents without taking into account possible backgrounds from the collisions.

In this study, we consider excited neutrino production in more detail (since excited spin-3/2 neutrinos are least studied compared to the excited spin-1/2 ones). We take into account the signals in different decay channels of excited neutrinos as well as the corresponding backgrounds at the International Linear Collider (ILC) [17] with $\sqrt{s} = 0.5$ TeV and Compact Linear Collider (CLIC) [18] with an optimal design energy of $\sqrt{s} = 3$ TeV. We present the missing transverse momentum distributions for single production of excited spin-3/2 and spin-1/2 neutrinos. The shape of these distributions would help to discriminate the signals from the background.

II. PHENOMENOLOGICAL CURRENTS

First, we consider the interaction between a spin-1/2 excited neutrino, a gauge boson ($V = \gamma$, Z, $W^\pm$), and the SM lepton described by the effective current:

$$J^\mu_{1/2} = \frac{g_e}{2\Lambda}\bar{u}(k, 1/2) i\sigma^{\mu\nu} q_\nu (1 - \gamma_5) f_V u(p, 1/2), \quad (1)$$

where Λ is the scale of new physics responsible for the new

*ocakir@mail.cern.ch
†aozansoy@mail.cern.ch

interactions, k, p and q are the four-momentum of the SM neutrino (electron), excited spin-1/2 neutrino and gauge boson γ, $Z(W^{\pm})$, respectively. g_e is the electromagnetic coupling constant, $g_e = \sqrt{4\pi\alpha}$. f_V is the electroweak coupling parameter corresponding to the vector boson V. In Eq. (1), $\sigma^{\mu\nu} = i(\gamma^\mu\gamma^\nu - \gamma^\nu\gamma^\mu)/2$ with γ^μ being the Dirac matrices. For an excited spin-1/2 neutrino, three decay channels are possible: radiative decay $\nu^* \to \nu\gamma$, neutral weak decay $\nu^* \to \nu Z$, and charged weak decay $\nu^* \to eW$. Neglecting the ordinary lepton masses we find decay widths as

$$\Gamma(l^{*(1/2)} \to lV) = \frac{\alpha m^{*3}}{4\Lambda^2} f_V^2 \left(1 - \frac{m_V^2}{m^{*2}}\right)^2 \left(1 + \frac{m_V^2}{2m^{*2}}\right), \quad (2)$$

where $f_\gamma = (f - f')/2$, $f_Z = (f\cot\theta_W + f'\tan\theta_W)/2$, $f_W = f/\sqrt{2}\sin\theta_W$, and m_V is the mass of the gauge boson. The parameters f and f' are determined by the composite dynamics, and they can be defined as q^2-dependent form factors. In the literature, they are often taken as $f = f' = 1$ or $f = -f' = 1$ with $\Lambda = m^*$. The total decay width of the excited spin-1/2 neutrino is $\Gamma = 3.4(6.9)$ GeV for $m^* = 0.5(1)$ TeV at $f = f' = 1$ and $\Lambda = m^*$. The branching ratios of the excited spin-1/2 neutrinos were presented in a previous work [19]. One may note that the electromagnetic interaction between excited neutrino and ordinary neutrino vanishes for $f = f'$. For $f = f' = 1$, the charged-current decays become dominant for higher mass values $m^* > 150$ GeV, while $f = -f' = 1$, and the branching ratio is $\sim$60% for the eW channel. Their relative importance depends on the gauge boson mass and couplings. At $f = -f' = 1$ the branchings will be 60% for the W channel, 12% for the Z channel, and 28% for the γ channel at higher excited spin-1/2 neutrino masses ($m^* >$ 500 GeV). Therefore, the signature of $\nu^* \to eW$ is preferable in both cases for the investigation of an excited neutrino in future linear collider experiments.

Second, the phenomenological currents for the interactions among the spin-3/2 excited neutrino, the gauge boson, and the SM lepton are given by

$$J_1^\mu = g_e u(k, 1/2)(c_{1V} - c_{1A}\gamma_5)u^\mu(p, 3/2), \quad (3)$$

$$J_2^\mu = \frac{g_e}{\Lambda} u(k, 1/2)q_\lambda\gamma^\mu(c_{2V} - c_{2A}\gamma_5)u^\lambda(p, 3/2), \quad (4)$$

$$J_3^\mu = \frac{g_e}{\Lambda^2} u(k, 1/2)q_\lambda i\sigma^{\mu\nu}q_\nu(c_{3V} - c_{3A}\gamma_5)u^\lambda(p, 3/2), \quad (5)$$

where $u^\mu(p, 3/2)$ represents the Rarita-Schwinger vector spinor [20], c_{iV} and c_{iA} are the vector and axial vector couplings, and the four momenta $q_\alpha = (p - k)_\alpha$ belongs to the vector boson. A spin-3/2 excited neutrino (ν^*) decays via a two-body process according to the phenomenological currents Eqs. (3)–(5). The radiative and weak decay widths of excited spin-3/2 neutrinos for three different currents can be written similar to that of the excited spin-3/2 electrons [14].

The relative importance of higher dimension operators is not essential when $\Lambda > m^*$. Taking $\Lambda = m^* = 0.5(1)$ TeV and $c_{iV} = c_{iA} = 0.5$, we find the total decay widths of the excited spin-3/2 neutrinos as $\Gamma_1 = 3.9(24.6)$ GeV, $\Gamma_2 = 2.7(22.2)$ GeV, and $\Gamma_3 = 0.23(0.48)$ GeV for the currents J_1, J_2, and J_3, respectively. For this parametrization the decay widths of the excited spin-3/2 neutrino with $c_{iV} = c_{iA} = 0.5$ for different mass values are identical to those of excited spin-3/2 electrons. One can note that even at $\Lambda = m^*$ and equal couplings, the values of the decay widths become different, because there are different radiative contributions for each current and the κ term affects these channels differently. For equal couplings $c_{iV} = c_{iA} = 0.5$ and $\Lambda = m^*$, the branchings for the weak decays corresponding to the current J_1 and J_2 become dominant for $m^* \gtrsim 200$ GeV. The radiative and the weak decay channels with the same couplings have equal probability for the current J_3 when $m^* \gtrsim 500$ GeV.

III. CROSS SECTIONS

The spin-1/2 and spin-3/2 excited neutrinos can be produced singly at future e^+e^- colliders, namely, ILC and CLIC. The Feynman diagrams contributing to the single production of excited neutrinos via the s-channel Z, the γ exchange, and the t-channel W exchange are shown in Fig. 1.

One may note that pair production of an excited neutrino in the t-channel W exchange is also possible with the currents given in the previous section. In the s-channel, pair production of excited neutrinos of any type could also be possible if their interactions with a photon and a Z boson are defined. On the other hand, the single production of ν_μ^* and ν_τ^* with the s-channel process is possible with and without the lepton flavor violating coupling.

Recently, spin-1/2 excited neutrinos have been studied at the ILC energy $\sqrt{s} = 0.5$ TeV in [19]. The $\nu^* \to eW$ signal has been searched for an easy identification and accurate measurements in a linear collider environment. The results show that the spin-1/2 excited neutrino can be probed up to the mass $m^* = 450$ GeV in the charged weak

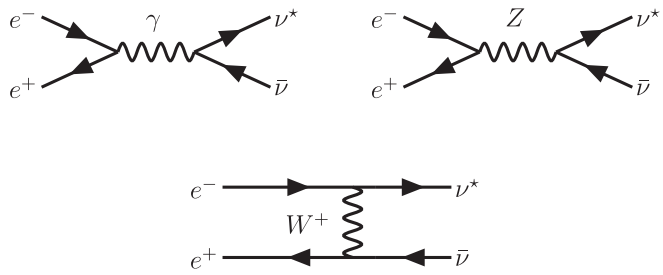

FIG. 1. Feynman diagrams for single excited spin-3/2 or spin-1/2 neutrino production in e^+e^- collisions.

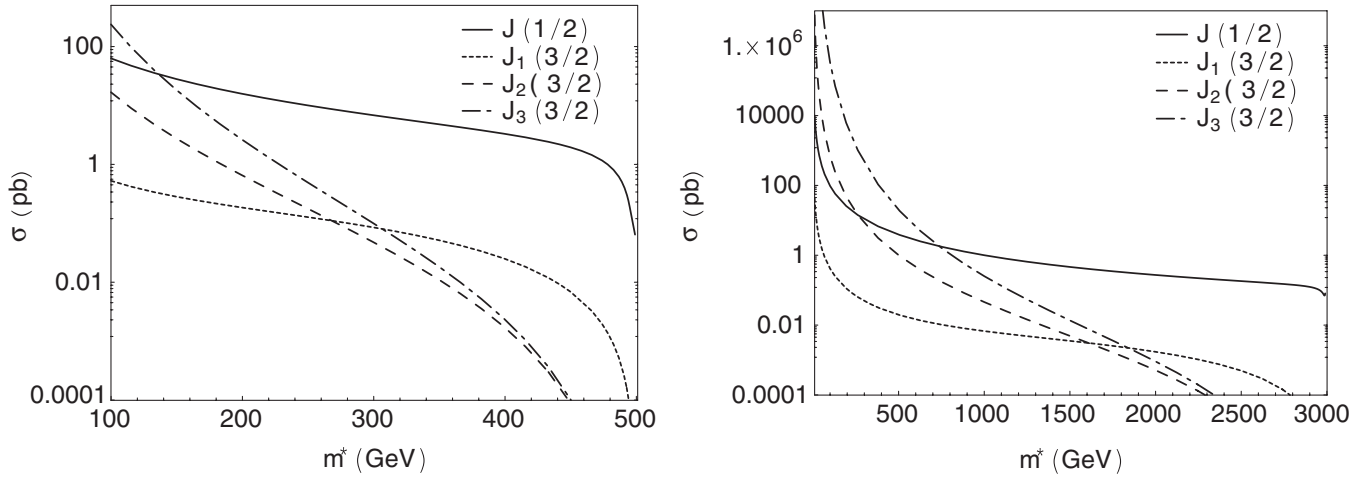

FIG. 2. Excited neutrino production cross section as a function of the mass at the ILC energy $\sqrt{s} = 0.5$ TeV (left panel) and CLIC energy $\sqrt{s} = 3$ TeV (right panel). Solid, dotted, dashed, and dot-dashed lines denote spin-1/2 current $J(1/2)$ for $f = -f' = 1$, and the spin-3/2 with J_1, J_2, J_3 currents for $c_{iV}^{\gamma} = c_{iA}^{\gamma} = 0.5$, respectively.

decay channel when the coupling parameters are taken as $f = f' = 0.1$ for $\Lambda = m^*$.

In order to calculate the cross sections for $e^+e^- \to \nu_e^* \bar{\nu}_e$ processes for three phenomenological spin-3/2 currents J_1, J_2, and J_3, we integrate over the Mandelstam variable t (or $\cos\theta$) of the diffential cross section

$$\frac{d\sigma}{dt} = \frac{g_e^2}{24 m^{*2} \pi s^2} \sum_{i \le j = 1,3} \frac{T_{ij}^{(k)}}{P_{ij}^{(k)}}, \tag{6}$$

where we use the expressions $T_{ij}^{(k)}$ and $P_{ij}^{(k)}$ as given in the Appendix. Total cross sections as a function of excited neutrino mass are presented in Figs. 2–4 at center of mass energies $\sqrt{s} = 0.5$ and $\sqrt{s} = 3$ TeV.

One can see from Figs. 2 and 3, the excited spin-3/2 neutrinos with current J_3 (having only c_i^{γ} or c_i^Z couplings) have a cross section larger than the other two currents (J_1 and J_2) when their mass is below 1.8 TeV and when they are produced at $\sqrt{s} = 3$ TeV. The cross section for the $\nu^*(J_3)$ via t-channel W exchange becomes more visible below $m^* < 1.4$ TeV, as shown in Fig. 4. Depending on the couplings c_{iV}, c_{iA} their (currents) relative importance (changes in the cross section for the interested mass range) becomes more pronounced compared to the excited spin-1/2 neutrinos.

In order to differentiate the spin-3/2 and spin-1/2 excited neutrino signals we plot the differential cross sections as a function of p_T in Figs. 5–7. The distributions of missing p_T for the single production of the spin-1/2 and

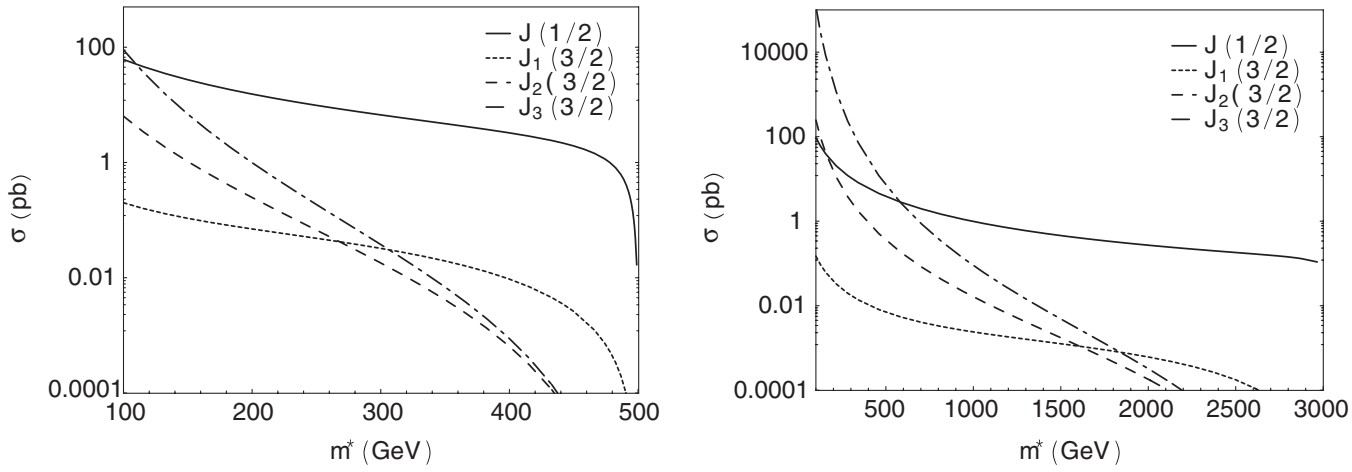

FIG. 3. Excited neutrino production cross section as a function of the mass at ILC with $\sqrt{s} = 0.5$ TeV (left panel) and CLIC with $\sqrt{s} = 3$ TeV (right panel). Solid, dotted, dashed, and dot-dashed lines denote spin-1/2 and spin-3/2 currents $J(1/2)$, J_1, J_2, and J_3 currents, respectively. Here, we take $f = f' = 1$ and $c_{iV}^Z = c_{iA}^Z = 0.5$ with $\Lambda = m^*$.

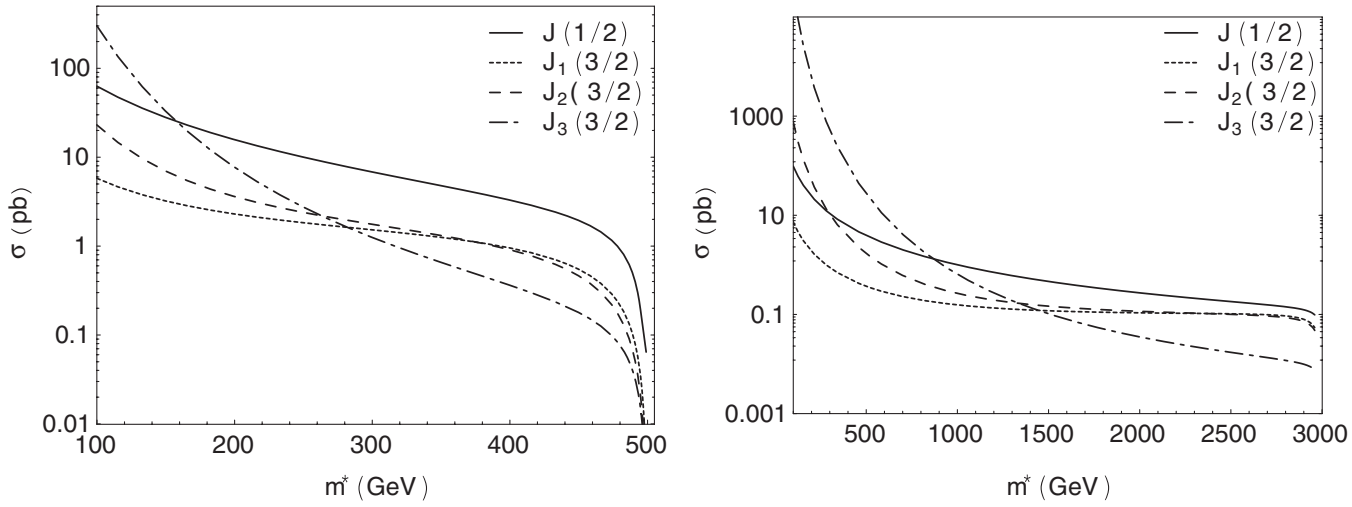

FIG. 4. Excited neutrino production cross section as a function of the mass at ILC (left panel) and CLIC (right panel). Solid, dotted, dashed, and dot-dashed lines denote spin-1/2 and spin-3/2 currents for $f = -f' = 1$ and $c_{iV}^W = c_{iA}^W = 0.5$, respectively. Here we take $\Lambda = m^*$.

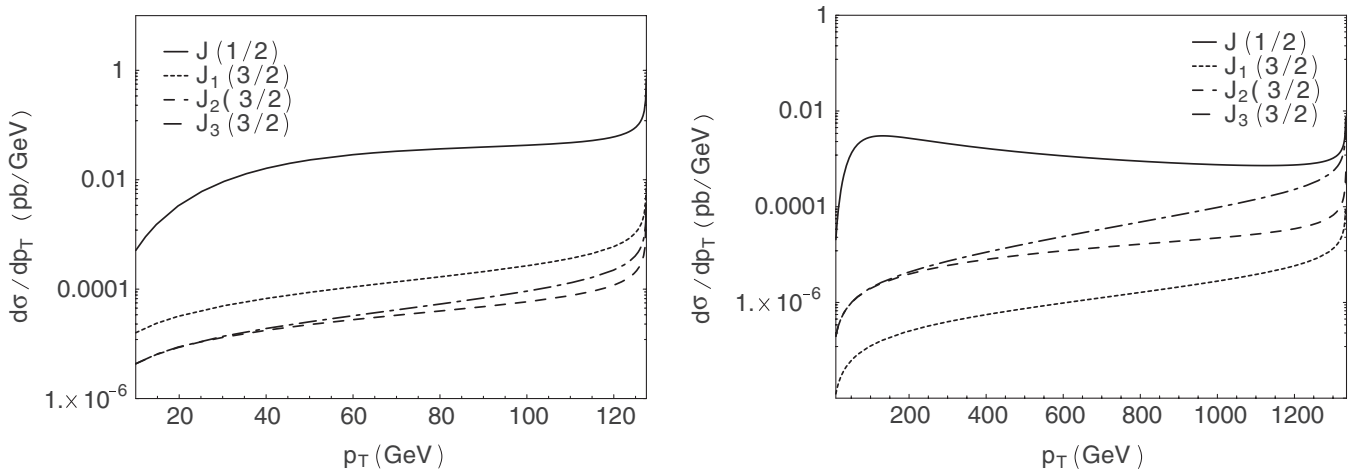

FIG. 5. The missing p_T distribution taking into account the coupling $c_{iV}^\gamma = c_{iA}^\gamma = 0.5$ for spin-3/2 currents and $f = -f' = 1$ for spin-1/2 currents with $\Lambda = m^*$, where $m^* = 350$ GeV for ILC and $m^* = 1$ TeV for CLIC.

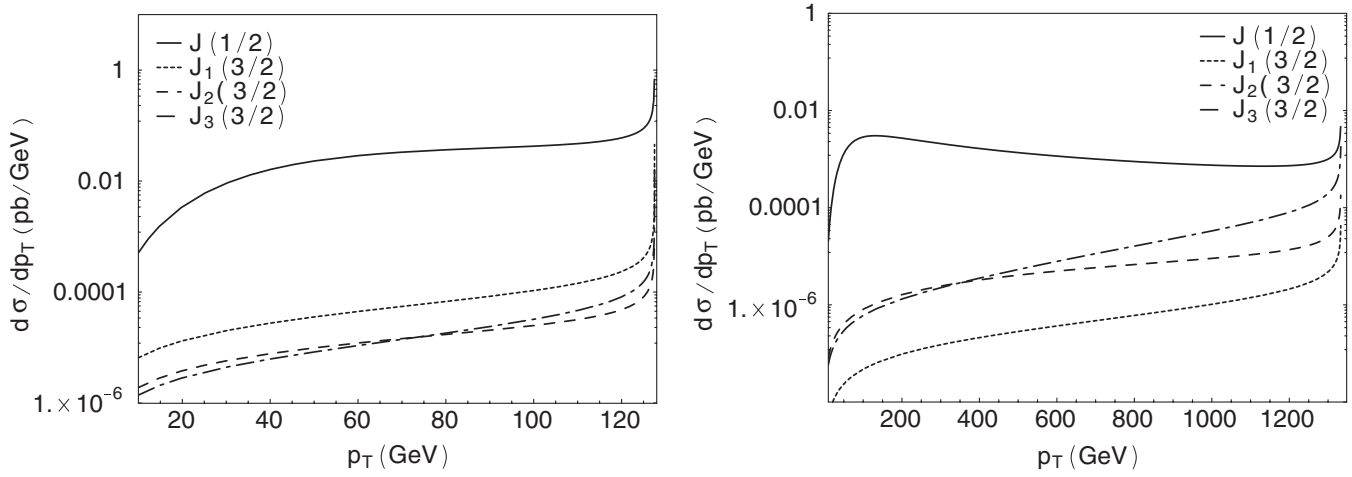

FIG. 6. The missing p_T distribution taking into account the coupling $c_{iV}^Z = c_{iA}^Z = 0.5$ for spin-3/2 currents and $f = f' = 1$ for spin-1/2 currents with $\Lambda = m^*$, where we take $m^* = 350$ GeV for ILC and $m^* = 1$ TeV for CLIC.

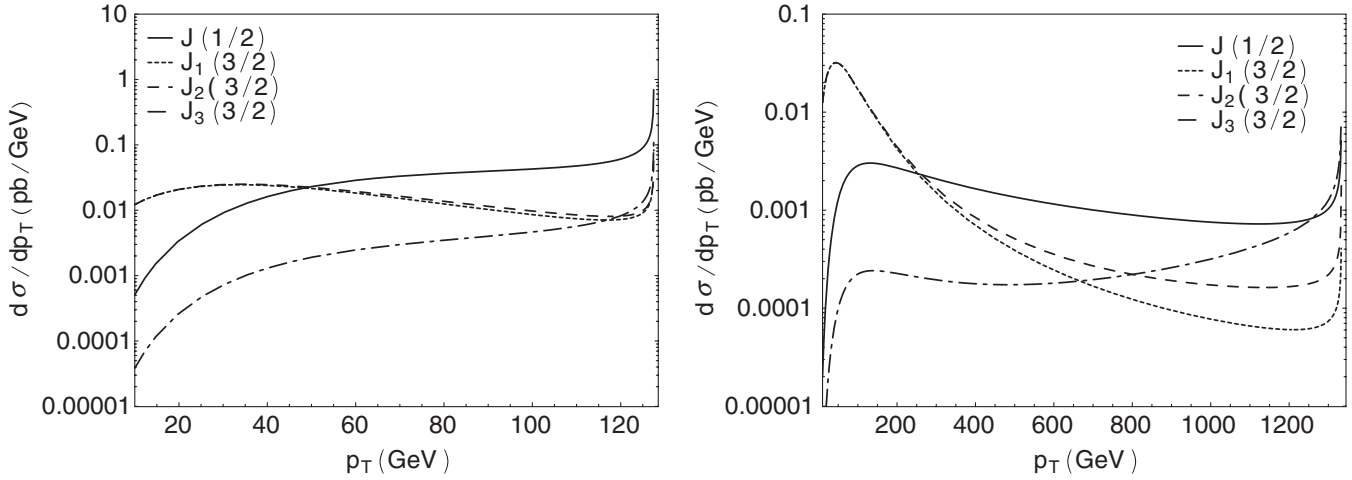

FIG. 7. The missing p_T distribution taking into account the coupling $c_{iV}^W = c_{iA}^W = 0.5$ for the currents $J_i(3/2)$ and $f = -f' = 1$ for $J(1/2)$ with $\Lambda = m^*$, where we used $m^* = 350$ GeV for ILC and $m^* = 1$ TeV for CLIC.

spin-3/2 excited neutrinos show different behaviors. Furthermore, the production of the excited spin-3/2 neutrino with J_3 interactions leads to different missing p_T distributions from the others (J_1 and J_2). Concerning the final state we consider three decay channels of signal $\nu^* \to \nu\gamma$, $\nu^* \to e^- W^+$, and $\nu^* \to \nu Z$ for an excited neutrino. These lead to the final state with $\gamma + \not{p}_T$, $e^\pm + 2j + \not{p}_T$, and $\ell^+\ell^- + \not{p}_T$ as shown in Table I. At the ILC energy of $\sqrt{s} = 500$ GeV, the shape of the missing transverse momentum $\not{p}_T$ for the signal concerning $e^+e^- \to W^+e^-\bar{\nu}$ process behaves different from that of the corresponding background in Fig. 8. However, at higher center of mass energies the currents $J_1(3/2)$ and $J_2(3/2)$ show similar behavior with the background especially at low $\not{p}_T$ region.

TABLE I. Final states for single excited neutrino production.

Decay mode	Production $e^+e^- \to \bar{\nu}\nu^*$
Radiative	$\bar{\nu}\nu\gamma$
Charged current	$\bar{\nu}e^-2j$
Neutral current	$\bar{\nu}\nu l^+l^-$

IV. ANALYSIS

In order to perceive the excited neutrino signals from the background we can put some cuts on the final state observable particles and a cut on the missing transverse momentum. In general, by applying suitable cuts the signal can be more pronounced over the background. For the acceptance of interested events we apply the following initial cuts:

$$p_T^{e,\gamma} > 20 \text{ GeV}, \tag{7}$$

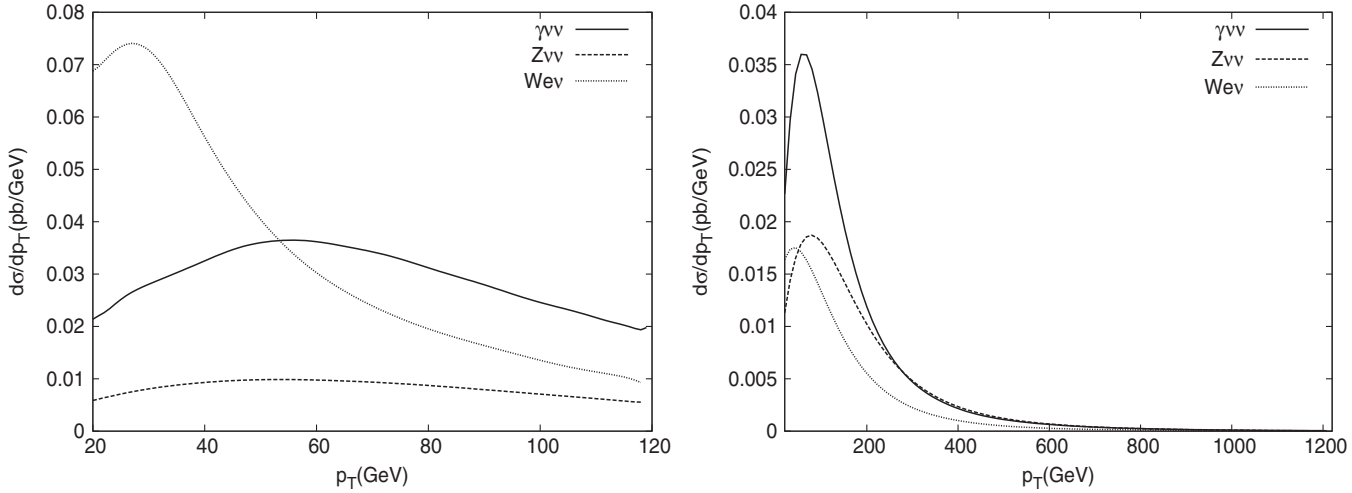

FIG. 8. Missing p_T distributions of background processes $e^+e^- \to \gamma\nu\bar{\nu}$, $e^+e^- \to Z\nu\bar{\nu}$, and $e^+e^- \to W^+e^-\bar{\nu}$ at ILC (left panel) and CLIC (right panel) energies.

$$|\eta_{e,\gamma}| < 2.5, \quad (8)$$

where p_T is the transverse momentum of the final state detectable particle, and η denotes pseudorapidity. Since the neutrino can be identified as the missing transverse momentum, we can also apply the same cut on the $\not{p}_T$. After applying these cuts we find the total cross section for the SM background as 1.062 (2.049) pb, 0.329 (2.083) pb, and 0.918 (0.463) pb at $\sqrt{s} = 0.5(3)$ TeV for the $e^+e^- \to \nu\bar{\nu}\gamma$, $e^+e^- \to \nu\bar{\nu}Z$, and $e^+e^- \to e^-\nu W^+$ processes, respectively. The program CALCHEP [21] is used to calculate the background cross sections with suitable cuts. In the analysis, we take into account one coupling c_{iV}, c_{iA} is kept free while the others are assumed to vanish. We present the

TABLE II. The cross section (in pb) for the spin-3/2 signal for $c_{iV}^{\gamma} = c_{iA}^{\gamma} = 0.5$ and spin-1/2 signal for $f = -f' = 1$ at $\sqrt{s} = 0.5$ TeV. Here we take $\Lambda = m^*$.

m^* (GeV)	$J(1/2)$	$J_1(3/2)$	$J_2(3/2)$	$J_3(3/2)$	$\sum_i J_i(3/2)$
200	5.36×10^{0}	1.85×10^{-1}	6.49×10^{-1}	2.60×10^{0}	3.43×10^{0}
250	3.21×10^{0}	1.27×10^{-1}	1.76×10^{-1}	4.90×10^{-1}	7.93×10^{-1}
300	2.05×10^{0}	8.50×10^{-2}	4.70×10^{-2}	9.90×10^{-2}	2.31×10^{-1}
350	1.43×10^{0}	5.10×10^{-2}	1.10×10^{-2}	1.80×10^{-2}	8.00×10^{-2}
400	9.50×10^{-1}	2.50×10^{-2}	1.17×10^{-3}	2.30×10^{-3}	2.85×10^{-2}
475	3.30×10^{-1}	1.80×10^{-3}	5.10×10^{-6}	5.40×10^{-6}	1.81×10^{-3}

TABLE III. The signal cross sections (in pb) for $c_{iV}^{\gamma} = c_{iA}^{\gamma} = 0.5$ and $f = -f' = 1$ for excited neutrinos at $\sqrt{s} = 3$ TeV. Here we take $\Lambda = m^*$.

m^* (GeV)	$J(1/2)$	$J_1(3/2)$	$J_2(3/2)$	$J_3(3/2)$	$\sum_i J_i(3/2)$
250	4.97×10^{0}	6.90×10^{-2}	1.73×10^{1}	1.35×10^{3}	1.37×10^{3}
500	1.13×10^{0}	2.00×10^{-2}	1.00×10^{0}	2.01×10^{1}	2.11×10^{1}
1000	2.80×10^{-1}	6.70×10^{-3}	4.60×10^{-2}	2.50×10^{-1}	3.03×10^{-1}
1500	1.29×10^{-1}	3.50×10^{-3}	4.90×10^{-3}	1.40×10^{-2}	2.24×10^{-2}
2000	7.60×10^{-2}	1.70×10^{-3}	5.10×10^{-4}	9.10×10^{-4}	3.12×10^{-3}
2500	5.00×10^{-2}	5.00×10^{-4}	2.10×10^{-5}	2.70×10^{-5}	5.48×10^{-4}
2750	4.20×10^{-2}	1.30×10^{-4}	1.14×10^{-6}	1.29×10^{-6}	1.32×10^{-4}

TABLE IV. The signal cross section (in pb) for $c_{iV}^{Z} = c_{iA}^{Z} = 0.5$ and $f = f' = 1$ for the excited neutrinos at $\sqrt{s} = 0.5$ TeV. Here we take $\Lambda = m^*$.

m^* (GeV)	$J(1/2)$	$J_1(3/2)$	$J_2(3/2)$	$J_3(3/2)$	$\sum_i J_i(3/2)$
200	5.68×10^{0}	7.00×10^{-2}	2.40×10^{-1}	9.90×10^{-1}	1.30×10^{0}
250	3.82×10^{0}	4.80×10^{-2}	6.70×10^{-2}	1.90×10^{-1}	3.05×10^{-1}
300	2.61×10^{0}	3.20×10^{-2}	1.80×10^{-2}	3.80×10^{-2}	8.80×10^{-2}
350	1.84×10^{0}	2.00×10^{-2}	4.20×10^{-3}	6.90×10^{-3}	3.11×10^{-2}
400	1.27×10^{0}	9.50×10^{-3}	6.40×10^{-4}	8.80×10^{-4}	1.10×10^{-2}
475	4.40×10^{-1}	6.80×10^{-4}	1.92×10^{-6}	2.07×10^{-6}	6.84×10^{-4}

TABLE V. The cross sections (in pb) for $c_{iV}^{Z} = c_{iA}^{Z} = 0.5$ and $f = f' = 1$ for excited neutrinos at $\sqrt{s} = 3$ TeV, and $\Lambda = m^*$.

m^* (GeV)	$J(1/2)$	$J_1(3/2)$	$J_2(3/2)$	$J_3(3/2)$	$\sum_i J_i(3/2)$
250	5.95×10^{0}	2.50×10^{-2}	6.15×10^{0}	4.80×10^{2}	4.86×10^{2}
500	1.50×10^{0}	7.00×10^{-3}	3.60×10^{-1}	7.16×10^{0}	7.53×10^{0}
1000	3.90×10^{-1}	2.40×10^{-3}	1.60×10^{-2}	9.00×10^{-2}	1.08×10^{-1}
1500	1.79×10^{-1}	1.30×10^{-3}	1.70×10^{-3}	4.80×10^{-3}	7.80×10^{-3}
2000	1.05×10^{-1}	6.10×10^{-4}	1.80×10^{-4}	3.20×10^{-4}	1.11×10^{-3}
2500	7.00×10^{-2}	1.80×10^{-4}	7.54×10^{-6}	9.74×10^{-6}	1.97×10^{-4}
2750	5.90×10^{-2}	4.80×10^{-5}	4.10×10^{-7}	4.60×10^{-7}	4.89×10^{-5}

TABLE VI. The signal and background cross sections (in pb) after the cuts. The signal cross section is given for $\Lambda = m^*$ and $c_{iV}^W = c_{iA}^W = 0.5$ for the spin-3/2 and $f = -f' = 1$ for the spin-1/2 at $\sqrt{s} = 0.5$ TeV. We have used $\Delta m = 50$ GeV.

m^* (GeV)	$J(1/2)$	$J_1(3/2)$	$J_2(3/2)$	$J_3(3/2)$	$\sum_i J_i(3/2)$	$\sigma_B(\Delta m)$
200	8.82×10^0	2.30×10^0	3.61×10^0	7.70×10^0	1.36×10^1	9.36×10^{-2}
250	5.81×10^0	1.83×10^0	2.39×10^0	2.75×10^0	6.97×10^0	9.12×10^{-2}
300	4.02×10^0	1.52×10^0	1.76×10^0	1.25×10^0	4.53×10^0	9.65×10^{-2}
350	2.82×10^0	1.26×10^0	1.32×10^0	6.60×10^{-1}	3.24×10^0	1.21×10^{-1}
400	1.97×10^0	9.50×10^{-1}	9.10×10^{-1}	3.60×10^{-1}	2.22×10^0	1.69×10^{-1}
475	6.70×10^{-1}	2.80×10^{-1}	2.10×10^{-1}	9.50×10^{-2}	5.85×10^{-1}	1.23×10^{-1}

TABLE VII. The signal and background cross sections (in pb) after the cuts. The cross section is given for $\Lambda = m^*$ and $c_{iV}^W = c_{iA}^W = 0.5$ for the spin-3/2 and $f = -f' = 1$ for the spin-1/2 signal at $\sqrt{s} = 3$ TeV.

m^* (GeV)	$J(1/2)$	$J_1(3/2)$	$J_2(3/2)$	$J_3(3/2)$	$\sum_i J_i(3/2)$	$\sigma_B(\Delta m)$
250	9.01×10^0	1.23×10^0	2.08×10^1	1.54×10^3	1.56×10^3	1.96×10^{-2}
500	2.35×10^0	3.70×10^{-1}	1.70×10^0	2.69×10^1	2.89×10^1	1.69×10^{-2}
1000	6.00×10^{-1}	1.60×10^{-1}	2.70×10^{-1}	6.50×10^{-1}	1.08×10^0	1.00×10^{-2}
1500	2.76×10^{-1}	1.20×10^{-1}	1.50×10^{-1}	1.00×10^{-1}	3.70×10^{-1}	1.83×10^{-1}
2000	1.62×10^{-1}	1.10×10^{-1}	1.20×10^{-1}	3.50×10^{-2}	2.65×10^{-1}	1.83×10^{-1}
2500	1.08×10^{-1}	1.00×10^{-1}	1.00×10^{-1}	1.70×10^{-2}	2.17×10^{-1}	1.83×10^{-1}
2750	9.00×10^{-2}	9.70×10^{-2}	9.00×10^{-2}	1.30×10^{-2}	2.00×10^{-1}	1.83×10^{-1}

signal cross sections in Tables II–V. In Tables VI and VII we give the cross sections for the signal and background in the relevant mass intervals.

We examine the single production of excited spin-3/2 and spin-1/2 neutrinos in the decay channels $\nu\gamma$, νZ, and $e^{\pm}W^{\mp}$. Concerning the final states we choose W boson decay hadronically and Z boson decay leptonically, because of the uncertainty from the neutrinos in the final state. The corresponding backgrounds can be studied by applying the cuts on the transverse momentum and pseudorapidities of final state leptons and jets. Furthermore, a way of extracting the excited neutrino signal is to impose a cut $|m_{ejj} - m^*| < 25$ GeV on the ejj invariant mass for the charged weak decay channels of ν^*. This cut can be relaxed for higher mass values of ν^*. For $m^* > 1.5$ TeV we apply an invariant mass cut $m_{ejj} > 1$ TeV for a clean detection of the signal.

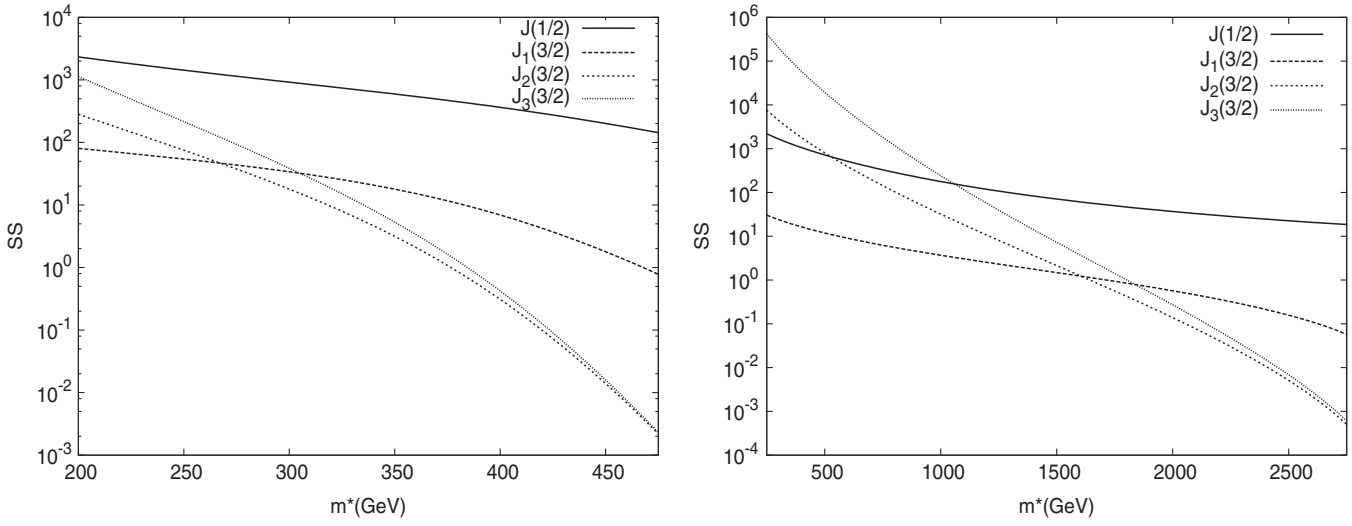

FIG. 9. Statistical significance as a function of excited neutrino mass for different spin-3/2 currents with the couplings $c_{iV}^{\gamma} = c_{iA}^{\gamma} = 0.5$, and spin-1/2 current with $f = -f' = 1$ at $\sqrt{s} = 0.5$ TeV (left panel) and $\sqrt{s} = 3$ TeV (right panel) using an integrated luminosity of $L_{\rm int} = 200$ fb^{-1} for ILC and $L_{\rm int} = 400$ fb^{-1} for CLIC energies.

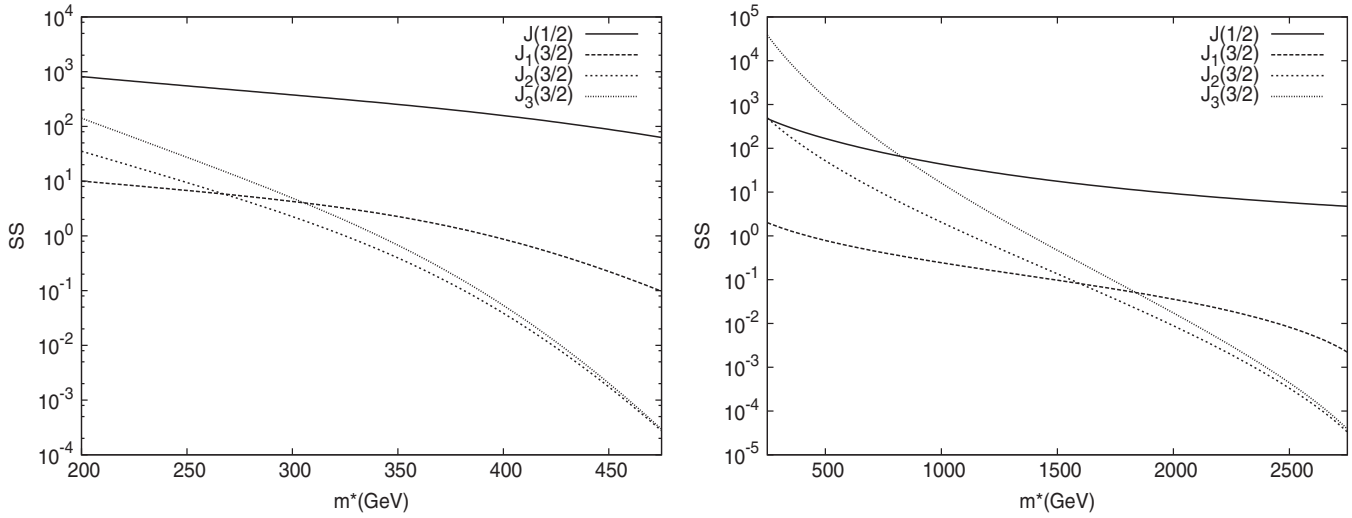

FIG. 10. Statistical significance as a function of excited neutrino mass for different spin-3/2 currents with the couplings $c_{iV}^{Z} = c_{iA}^{Z} = 0.5$, and spin-1/2 current with $f = f' = 1$ at $\sqrt{s} = 0.5$ TeV (left panel) and $\sqrt{s} = 3$ TeV (right panel) using an integrated luminosity of $L_{\text{int}} = 200$ fb^{-1} for ILC and $L_{\text{int}} = 400$ fb^{-1} for CLIC energies.

For the analysis we define the statistical significance (SS) of the signal as

$$SS = \frac{\sigma_S}{\sqrt{\sigma_B}}\sqrt{\epsilon L},$$

where L_{int} is the integrated luminosity of the collider and ϵ is the efficiency to detect the signal in the chosen channel. In the $\nu^* \to \nu\gamma$ and $\nu^* \to \nu Z$ channels, we have used the cross section for the signal and background to calculate the significance. Requiring $SS > 3$ the attainable mass range covers up to $m^* \approx 1.3$–1.5 TeV (as seen from Figs. 9–11) for an excited spin-3/2 neutrino at CLIC with $\sqrt{s} = 3$ TeV. For the $\nu^* \to eW$ channel, the values of the significance are evaluated at each mass value (invariant mass intervals) and the results are presented in Fig. 11 for the discovery reach for excited spin-3/2 and spin-1/2 neutrinos. A smaller coupling $c_{iV}^{W} = c_{iA}^{W} = 0.05$ can be reached in the $\nu^* \to eW$ channel. At the ILC, the attainable mass ranges for spin-3/2 charged currents can be covered up to the center of mass energy.

Here, we have used three different phenomenological currents for the spin-3/2 excited neutrino interactions. We also calculate all their contributions for the same value of the couplings. The results are given in the last column of Tables II–V and the sixth columns of Tables VI and VII. The contributions to the cross section from different cur-

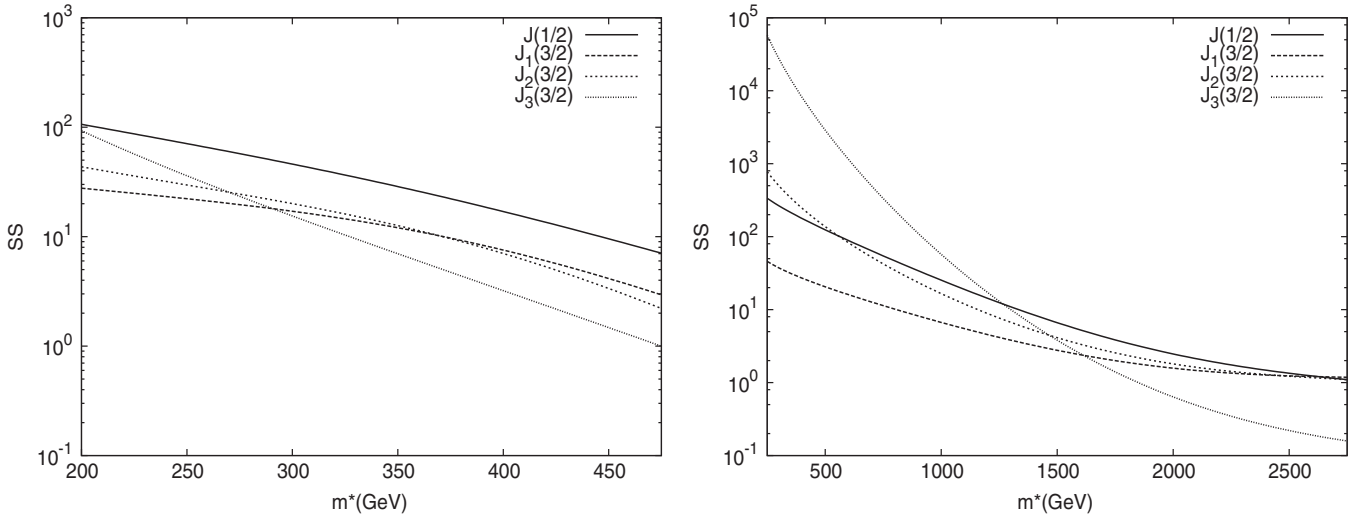

FIG. 11. Statistical significance as a function of excited neutrino mass for different spin-3/2 currents with the couplings $c_{iV}^{W} = c_{iA}^{W} = 0.05$, and spin-1/2 current with $f = -f' = 1$ at $\sqrt{s} = 0.5$ TeV (left panel) and $\sqrt{s} = 3$ TeV (right panel) using an integrated luminosity of $L_{\text{int}} = 200$ fb^{-1} for ILC and $L_{\text{int}} = 400$ fb^{-1} for CLIC energies.

rents can be comparable at some parameter space. Their relative importance will depend on the excited neutrino mass value and the couplings, in case the contributions from different currents present at the same time also change the significance of the signal in the interested channels.

V. CONCLUSION

We consider only the gauge interactions of excited spin-1/2 and spin-3/2 particles with the SM particles. Our analysis shows that spin-3/2 excited neutrinos can be easily separated from the spin-1/2 ones by examining both the transverse momentum distributions of final state visible and invisible particles when they produce singly at future linear colliders. If polarized e^+ and e^- beams are used the chiral structure of the couplings can be identified and more precise measurements can be performed at the ILC and CLIC environments.

Since the currents for spin-3/2 have unknown couplings, it is reasonable to treat one current at a time by neglecting the interference effects for the sake of simplicity. However, we also mention that in a full fledged calculation (e.g., by helicity methods or others), the interference effects could be important in some parameter space.

Excited neutrinos can come in three families, ν_e^*, ν_μ^*, and ν_τ^*. This study for ν_e^* can also be enlarged by applying similar analysis to the excited muon neutrinos and tau neutrinos at the future high energy linear colliders, and their signal distribution would be very different from that for ν_{e^*} when they are produced in the t-channel diagrams with the flavor violating coupling.

ACKNOWLEDGMENTS

We thank A. Belyaev and A. Pukhov for discussions on the CALCHEP implementation. The authors acknowledge the support from the CERN TH Division. A. O. would like to thank the members of the Nuclear Theory Group of the University of Wisconsin for their hospitality. A. O. acknowledges the support through the Scientific and Technical Research Council (TUBITAK) BIDEB-2214. This work was partially supported by the Turkish State Planning Organisation (DPT) under Grant No. DPT-2006K-120470.

APPENDIX

In Eq. (6) the operator terms $T_{ij}^{(1)}$ and propogators $P_{ij}^{(1)}$ for the spin-3/2 excited neutrino interaction current J_1 are given as

$$
\begin{aligned}
T_{11}^{(1)} &= -g_e^2(c_{1A}^{\gamma\,2} + c_{1V}^{\gamma\,2})(m^{*2} - s)(-t(s+t) + m^{*2}(2s+t)),\\
T_{12}^{(1)} &= [-g_e g_z(m_Z^2 - s)(c_{1A}^{\gamma}(c_{1V}^{Z} c_A^f m^{*2} s(m^{*2} - s - 2t) + c_{1A}^{Z} c_V^f(st(s+t) + m^{*4}(2s+t) - m^{*2}(2s^2 + 2st + t^2)))\\
&\quad + c_{1V}^{\gamma}(c_{1A}^{Z} c_A^f m^{*2} s(m^{*2} - s - 2t) + c_{1V}^{Z} c_V^f(st(s+t) + m^{*4}(2s+t) - m^{*2}(2s^2 + 2st + t^2))))/2,\\
T_{13}^{(1)} &= [-g_e g_w(c_{1A}^{W} - c_{1V}^{W})(c_{1A}^{\gamma} - c_{1V}^{\gamma})((m^{*4} + st)(s+t) - m^{*2}(s^2 + t^2))]/4\sqrt{2},\\
T_{22}^{(1)} &= [-g_z^2(4c_{1A}^{Z} c_{1V}^{Z} c_A^f c_V^f m^{*2} s(m^{*2} - s - 2t) + (c_{1A}^{Z\,2} + c_{1V}^{Z\,2})((c_A^{f2} + c_V^{f2})(m^{*2} - s)(-t(s+t) + m^{*2}(2s+t)))]/4,\\
T_{23}^{(1)} &= [-g_e g_w((c_{1A}^{W} - c_{1V}^{W})(c_{1A}^{Z} - c_{1V}^{Z})(c_A^f + c_V^f)(m_z^2 - s)((m^{*4} + st)(s+t) - m^{*2}(s^2 + t^2)))]/8\sqrt{2},\\
T_{33}^{(1)} &= [-g_w^2((c_{1A}^{W\,2} + c_{1V}^{W\,2})(-m^{*2} + t)(s(s+t) - m^{*2}(s+2t))) + 2c_{1A}^{W} c_{1V}^{W} m^{*2}(m^{*2} - 2s - t)t]/4,
\end{aligned}
$$

and

$$
P_{11}^{(1)} = s^2, \qquad P_{12}^{(1)} = s(m_z^4 + s^2 + m_z^2(-2s + \Gamma_Z^2)), \qquad P_{13}^{(1)} = s(m_w^2 - t),
$$

$$
P_{22}^{(1)} = (m_z^4 + s^2 + m_z^2(-2s + \Gamma_Z^2)),
$$

$$
P_{23}^{(1)} = (m_w^2 - t)(m_z^4 + s^2 + m_z^2(-2s + \Gamma_Z^2)), \qquad P_{33}^{(1)} = (m_w^2 - t)^2.
$$

The $T_{ij}^{(2)}$ and $P_{ij}^{(2)}$ terms for the current J_2 are given by

$$T_{11}^{(2)} = -g_e^2(c_{2A}^{\gamma\,2} + c_{2V}^{\gamma\,2})(m^{*2} - s)^2(-s^2 - 2st - 2t^2 + m^{*2}(s + 2t))/2,$$

$$T_{12}^{(2)} = [g_e g_z(m^{*2} - s)^2(-m_z^2 + s)(c_{2A}^{\gamma}(c_{2V}^{Z} c_A^f s(m^{*2} - s - 2t) + c_{2A}^{Z} c_V^f(-s^2 - 2st - 2t^2 + m^{*2}(s + 2t))) + c_{2V}^{\gamma}(c_{2A}^{Z} c_A^f s(m^{*2} - s - 2t) + c_{2V}^{Z} c_V^f(-s^2 - 2st - 2t^2 + m^{*2}(s + 2t))))]/4,$$

$$T_{13}^{(2)} = [-g_e g_w(c_{2A}^{W} + c_{2V}^{W})(c_{2A}^{\gamma} + c_{2V}^{\gamma})(m^{*2} - s - t)(s + t)(m^{*4} - st - m^{*2}(s + t))]/4\sqrt{2},$$

$$T_{22}^{(2)} = [-g_z^2(m^{*2} - s)^2(-4c_{2A}^{Z} c_{2V}^{Z} c_A^f c_V^f s(-m^{*2} + s + 2t) + (c_{2A}^{Z\,2} + c_{2V}^{Z\,2})((c_A^{f2} + c_V^{f2})(-s^2 - 2st - 2t^2 + m^{*2}(s + 2t))))]/8,$$

$$T_{23}^{(2)} = [-g_z g_w((c_{2A}^{W} + c_{2V}^{W})(c_{2A}^{Z} + c_{2V}^{Z})(c_A^f + c_V^f)(m_z^2 - s)(s + t)(-m^{*2} + s + t)(s + t)(-m^{*4} + st + m^{*2}(s + t)))]/8\sqrt{2},$$

$$T_{33}^{(2)} = [-g_w^2((-m^{*2} + t)^2(2c_{2A}^{W} c_{2V}^{W}(m^{*2} - 2s - t)t + (c_{2A}^{W\,2} + c_{2V}^{W\,2})(-2s^2 - 2st - t^2 + m^{*2}(2s + t))))]/4,$$

and

$$P_{11}^{(2)} = s^2\Lambda^2, \qquad P_{12}^{(2)} = s(m_z^4 + s^2 + m_z^2(-2s + \Gamma_Z^2))\Lambda^2, \qquad P_{13}^{(2)} = s(m_w^2 - t)\Lambda^2,$$

$$P_{22}^{(2)} = (m_z^4 + s^2 + m_z^2(-2s + \Gamma_Z^2))\Lambda^2,$$

$$P_{23}^{(2)} = (m_w^2 - t)(m_z^4 + s^2 + m_z^2(-2s + \Gamma_Z^2))\Lambda^2, \qquad P_{33}^{(2)} = (m_w^2 - t)^2\Lambda^2.$$

The $T_{ij}^{(3)}$ and $P_{ij}^{(3)}$ terms for the current J_3 are given by

$$T_{11}^{(3)} = -g_e^2(c_{3A}^{\gamma\,2} + c_{3V}^{\gamma\,2})(m^{*2} - s)^2(m^{*4} + 2t(s + t) - m^{*2}(s + 2t))/2,$$

$$T_{12}^{(3)} = [-g_e g_z(m^{*2} - s)^2(-m_z^2 + s)(c_{3A}^{\gamma}(c_{3V}^{Z} c_A^f m^{*2}(m^{*2} - s - 2t) - c_{3A}^{Z} c_V^f(m^{*4} + 2t(s + t) - m^{*2}(s + 2t))) + c_{3V}^{\gamma}(c_{3A}^{Z} c_A^f m^{*2}(m^{*2} - s - 2t) - c_{3V}^{Z} c_V^f(m^{*4} + 2t(s + t) - m^{*2}(s + 2t))))]/4,$$

$$T_{13}^{(3)} = [-g_e g_w(c_{3A}^{W} - c_{3V}^{W})(c_{3A}^{\gamma} - c_{3V}^{\gamma})(m^{*2} - s - t)t(m^{*2}(s - t) + st + m^{*2}(-s + t))]/4\sqrt{2},$$

$$T_{22}^{(3)} = [-g_z^2(m^{*2} - s)^2 s(4c_{3A}^{Z} c_{3V}^{Z} c_A^f c_V^f m^{*2}(-m^{*2} + s + 2t) + (c_{3A}^{Z\,2} + c_{3V}^{Z\,2})((c_A^{f2} + c_V^{f2})(m^{*4} + 2t(s + t) - m^{*2}(s + 2t)))]/8,$$

$$T_{23}^{(3)} = [g_z g_w s((c_{3A}^{W} - c_{3V}^{W})(c_{3A}^{Z} - c_{3V}^{Z})(c_A^f + c_V^f)(m_z^2 - s)t(-m^{*2} + s + t)(-m^{*2}(s - t) + st + m^{*2}(-s + t)))]/8\sqrt{2},$$

$$T_{33}^{(3)} = [-g_w^2((-m^{*2} + t)^2 t(2c_{3A}^{W} c_{3V}^{W} m^{*2}(-m^{*2} + 2s + t) + ((c_{3A}^{W\,2} + c_{3V}^{W\,2})(m^{*4} + 2s(s + t) - m^{*2}(2s + t))))]/4,$$

and

$$P_{11}^{(3)} = s\Lambda^4, \qquad P_{12}^{(3)} = (m_z^4 + s^2 + m_z^2(-2s + \Gamma_Z^2))\Lambda^4, \qquad P_{13}^{(3)} = (t - m_w^2)\Lambda^4,$$

$$P_{22}^{(3)} = (m_z^4 + s^2 + m_z^2(-2s + \Gamma_Z^2))\Lambda^4, \qquad P_{23}^{(3)} = (t - m_w^2)(m_z^4 + s^2 + m_z^2(-2s + \Gamma_Z^2))\Lambda^4, \qquad P_{33}^{(3)} = (t - m_w^2)^2\Lambda^4.$$

[1] H. Terazawa, Y. Chikashige, and K. Akama, Phys. Rev. D **15**, 480 (1977); Y. Ne'eman, Phys. Lett. **82B**, 69 (1979); H. Terazawa, M. Yasue, K. Akama, and M. Hayashi, Phys. Lett. **112B**, 387 (1982).

[2] F. M. Renard, Nuovo Cimento A **77**, 1 (1983); E. J. Eichten, K. D. Lane, and M. E. Peskin, Phys. Rev. Lett. **50**, 811 (1983); A. De Rujula, L. Maiani and, and R. Petronzio, Phys. Lett. **140B**, 253 (1984); J. Kühn and P. M. Zerwas, Phys. Lett. **147B**, 189 (1984).

[3] J. Leite Lopes, J. A. Martins Simoes, and D. Spehler, Phys. Lett. **94B**, 367 (1980); Phys. Rev. D **23**, 797 (1981); **25**, 1854 (1982).

[4] Y. Tosa and R. E. Marshak, Phys. Rev. D **32**, 774 (1985).

[5] D. Z. Freedman, P. van Nieuwenhuizen, and S. Ferrara, Phys. Rev. D **13**, 3214 (1976).

[6] R. Walsh and A. J. Ramalho, Phys. Rev. D **67**, 097702 (2003).

[7] P. Achard *et al.*, Phys. Lett. B **568**, 23 (2003); **531**, 39 (2002).
[8] F. D. Aaron *et al.*, Phys. Lett. B **663**, 382 (2008).
[9] U. Baur, M. Spira, and P. M. Zerwas, Phys. Rev. D **42**, 815 (1990).
[10] O. J. P. Eboli and S. M. Lietti, Phys. Rev. D **65**, 075003 (2002).
[11] O. Cakir *et al.*, Eur. Phys. J. C **32**, s1 (2004).
[12] K. Hagiwara, D. Zeppenfeld, and S. Komamiya, Z. Phys. C **29**, 115 (1985).
[13] F. Boudjema and A. Djouadi, Phys. Lett. B **240**, 485 (1990); F. Boudjema, A. Djouadi, and J. L. Kneur, Z. Phys. C **57**, 425 (1993).
[14] O. Cakir and A. Ozansoy, Phys. Rev. D **77**, 035002 (2008).
[15] S. R. Choudhury, R. G. Ellis, and G. C. Joshi, Phys. Rev. D **31**, 2390 (1985).
[16] F. M. L. Almeida *et al.*, Phys. Rev. D **53**, 3555 (1996).
[17] G. A. Loew, Report from the ILC technical review committee, SLAC Report No. Slac-pub-10024, 2003. A comprehensive information about the future linear colliders can be found at http://www.linearcollider.org.
[18] R. W. Assmann *et al.* (The CLIC Study Team), CERN Report No. CERN-2000-008, Geneva, 2000; E. Accomando *et al.* (CLIC Physics Working Group), arXiv:hep-ph/0412251.
[19] O. Cakir, A. Yilmaz, and S. Sultansoy, Phys. Rev. D **70**, 075011 (2004); O. Cakir, I. Turk Cakir, and Z. Kirca, Phys. Rev. D **70**, 075017 (2004).
[20] W. Rarita and J. Schwinger, Phys. Rev. **60**, 61 (1941).
[21] A. Pukhov *et al.*, arXiv:hep-ph/9908288; A. Pukhov, arXiv:hep-ph/0412191.